nanomaterials

MDPI

Article

New Perspectives on the Electronic and Geometric Structure of $Au_{70}S_{20}(PPh_3)_{12}$ Cluster: Superatomic-Network Core Protected by Novel $Au_{12}(\mu_3\text{-}S)_{10}$ Staple Motifs

Zhimei Tian [1,2], Yangyang Xu [3] and Longjiu Cheng [1,4,*]

1 Department of Chemistry, Anhui University, Hefei 230601, China
2 School of Chemistry and Materials Engineering, Fuyang Normal University, Fuyang 236037, China
3 School of Social and Public Administration, East China University of Science and Technology, Shanghai 200237, China
4 Anhui Province Key Laboratory of Chemistry for Inorganic/Organic Hybrid Functionalized Materials, Anhui University, Hefei 230601, China
* Correspondence: clj@ustc.edu; Tel.: +86-0551-63861279

Received: 5 July 2019; Accepted: 30 July 2019; Published: 6 August 2019

Abstract: In order to increase the understanding of the recently synthesized $Au_{70}S_{20}(PPh_3)_{12}$ cluster, we used the divide and protect concept and superatom network model (SAN) to study the electronic and geometric of the cluster. According to the experimental coordinates of the cluster, the study of $Au_{70}S_{20}(PPh_3)_{12}$ cluster was carried out using density functional theory calculations. Based on the superatom complex (SAC) model, the number of the valence electrons of the cluster is 30. It is not the number of valence electrons satisfied for a magic cluster. According to the concept of divide and protect, $Au_{70}S_{20}(PPh_3)_{12}$ cluster can be viewed as Au-core protected by various staple motifs. On the basis of SAN model, the Au-core is composed of a union of 2e-superatoms, and 2e-superatoms can be Au_3, Au_4, Au_5, or Au_6. $Au_{70}S_{20}(PPh_3)_{12}$ cluster should contain fifteen 2e-superatoms on the basis of SAN model. On analyzing the chemical bonding features of $Au_{70}S_{20}(PPh_3)_{12}$, we showed that the electronic structure of it has a network of fifteen 2e-superatoms, abbreviated as 15 × 2e SAN. On the basis of the divide and protect concept, $Au_{70}S_{20}(PPh_3)_{12}$ cluster can be viewed as $Au_{46}{}^{16+}[Au_{12}(\mu_3\text{-}S)_{10}{}^{8-}]_2[PPh_3]_{12}$. The $Au_{46}{}^{16+}$ core is composed of one $Au_{22}{}^{12+}$ innermost core and ten surrounding 2e-Au_4 superatoms. The $Au_{22}{}^{12+}$ innermost core can either be viewed as a network of five 2e-Au_6 superatoms, or be considered as a 10e-superatomic molecule. This new segmentation method can properly explain the structure and stability of $Au_{70}S_{20}(PPh_3)_{12}$ cluster. A novel extended staple motif $[Au_{12}(\mu_3\text{-}S)_{10}]^{8-}$ was discovered, which is a half-cage with ten μ_3-S units and six teeth. The six teeth staple motif enriches the family of staple motifs in ligand-protected Au clusters. $Au_{70}S_{20}(PPh_3)_{12}$ cluster derives its stability from SAN model and aurophilic interactions. Inspired by the half-cage motif, we design three core-in-cage clusters with cage staple motifs, $Cu_6@Au_{12}(\mu_3\text{-}S)_8$, $Ag_6@Au_{12}(\mu_3\text{-}S)_8$ and $Au_6@Au_{12}(\mu_3\text{-}S)_8$, which exhibit high thermostability and may be synthesized in future.

Keywords: $Au_{70}S_{20}(PPh_3)_{12}$ cluster; superatom network model; electronic structure; geometric structure

1. Introduction

Due to the applications in catalysis, optoelectronics, and photoluminescence, ligand-protected gold (Au-L) nanoclusters have drew much attention in both experiment [1–6] and theory [7–11].

The synthesis of Au-L clusters contributes much to many areas of science and technology because they have interesting structures [12,13]. In the past few years, the metalloid thiolate-protected Au nanoclusters with μ_3-S atoms have extended the family and potential applications of Au-L clusters. The experimentally determined metalloid Au-L clusters containing one or two μ_3-S include $Au_{21}S(SR)_{15}$ [14], $Au_{30}S(SR)_{18}$ [15,16], $Au_{38}S_2(SR)_{20}$ [17], and $Au_{103}S_2(SR)_{41}$ clusters [18], while $Au_{30}S_2(SR)_{18}$ cluster is a structure from theoretical prediction [19]. A large metalloid $Au_{108}S_{24}(PPh_3)_{16}$ cluster with 24 μ_3-S has been revealed, which consists of an octahedral Au_{44} core, an $Au_{48}S_{24}$ shell and 16 $Au(PPh_3)$ elements [20]. Very recently, Kenzler et al. has synthesized an intermediate size metalloid gold cluster $Au_{70}S_{20}(PPh_3)_{12}$, revealing an Au_{22} core surrounded by the $Au_{48}S_{20}(PPh_3)_{12}$ shell [21]. According to their report, Au_4S_4 unit is a central structural motif in the shell and they suggest that they could not elucidate a definite superatom character or distinct shell structure in the cluster. Thus, it is necessary to give a detailed study for the cluster, which may help to deeply understand the stability and structural nature of the cluster.

Häkkinen et al. proposed the divide-and-protect concept [22], and Au-L clusters are composed of Au-core and staple motifs; Au-core is protected by staple motifs. The concept has been widely used to predict and analyze the structures of Au-L clusters [23–32]. The idea of staple motif has been introduced since the synthesis of $Au_{102}(SR)_{44}$ cluster, and Jadzinsky et al. termed it [1]. To date, various forms of staple motifs (-SR-$(AuSR)_{x-}$) present in experimentally determined and theoretically predicted Au-L clusters. Monomer and dimer staple motifs present in $Au_{102}(SR)_{44}$ cluster [1]. Dimer staple motif also presents in $Au_{36}(SR)_{24}$ cluster [33]. Bridging -SR ligand and trimer staple motif exist in $Au_{23}(SR)_{16-}$ cluster [4]. In addition, gold-thiolate rings present in $Au_{20}(SR)_{16}$ and $Au_{22}(SR)_{18}$ clusters [8,34]. The protecting motifs include Au and SR, or only SR; moreover, they have two legs. We have predicted a tridentate staple motif with three S legs in the synthesized $Au_{30}S(SR)_{18}$ cluster before [19]. According to the superatom complex (SAC) concept proposed by Häkkinen et al [35], the number of valence electrons (V) for $Au_mS_n(SR)_p{}^q$ cluster is computed as bellow: $V = m - 2n - p - q$, in which m, n and p are the numbers of Au, S and SR, respectively, whereas q is the charge of the cluster. The super shells for spherical Au clusters is $|1S^2|1P^6|1D^{10}|2S^21F^{14}|2P^61G^{18}|\ldots$ (*S–P–D–F–G–H–* denote angular-momentum characters), corresponded to magic numbers 2, 8, 18, 34, 58, ... According to SAC model, clusters with valence electrons 2, 8, 18, 34, 58, . . . present special stability and they are magic number clusters. The theoretically predicted $Au_{12}(SR)_9{}^+$ and $Au_8(SR)_6$ are 2e magic clusters. $Au_{25}(SR)_{18}{}^-$, $Au_{44}(SR)_{28}{}^{2-}$ and $Au_{102}(SR)_{44}$ are 8e, 18e and 58e magic number clusters, respectively. Cheng et al. introduced the superatom-network (SAN) model, which has been used to explore the stability of $Au_{18}(SR)_{14}$, $Au_{20}(SR)_{16}$, $Au_{24}(SR)_{20}$, $Au_{44}(SR)_{28}$ and $Au_{22}(SR)_{18}$ clusters [8,36,37]. Based on the concept of SAN model, the Au-core of Au-L cluster can be viewed as a network of 2e Au_n (n = 3, 4, 5 or 6) superatoms. The interactions between the superatoms are main non-bond interactions.

Here, we investigate the electronic and geometric structure of $Au_{70}S_{20}(PPh_3)_{12}$ to obtain deep understanding of it. Based on the superatom complex (SAC) model, this cluster is a 30e compound [35]. The number of valence electrons for $Au_{70}S_{20}(PCH_3)_{12}$ cluster does not satisfy the magic number electrons of SAC model. Kenzler et al. reported that the Au core of $Au_{70}S_{20}(PPh_3)_{12}$ cluster is Au_{22}, and the protecting tetrahedral shell is composed of four Au_4S_4 units, four S atoms and 32 gold atoms, and no staple motif presents [21]. We are interested in the synthesized $Au_{70}S_{20}(PPh_3)_{12}$ cluster, which has 20 μ_3-S atoms. Now that the number of the valence electrons does not satisfy the SAC model, why it is stable? How do the 20 μ_3-S atoms protect the Au-core? What are the protecting motifs of the cluster? With these questions in mind, we tried to analyze the electronic and geometric structure of the cluster using existing theories and models. This work attempts to explain the structure and properties from a new perspective.

2. Materials and Methods

We start from the experimental structure of $Au_{70}S_{20}(PPh_3)_{12}$ determined as reported by Kenzler et al [21] and the total charge is set to zero. Considering the calculation amount, we used CH_3 instead

of all the Ph ligands, and the structure was then relaxed using the Gaussian 09 software (Revision B 01; *Gaussian*, Inc., Wallingford, CT, USA) [38]. Density-functional theory (DFT) calculations were employed to optimize the geometric structure using Perdew–Burke–Ernzerhof (PBE0) functional [39]. The basis set of Au element is Lanl2dz, while 6-31G * is used for S, P, C, H elements. The molecular orbital (MO) and natural bond orbital (NBO) calculations of Au cores were also carried out at the same level, whereas the basis set of Au element was Lanl2mb. The adaptive natural density partitioning (AdNDP) method was used to analyze the chemical bonding patterns [40]. MOLEKEL software (version 5.4.0.8, Swiss National Supercomputing Centre, Manno, Switzerland) [41] was used to view the chemical bonding patterns. The superatom-network (SAN) model was taken to analyze the chemical bonds in $Au_{70}S_{20}(PPh_3)_{12}$ cluster [36].

3. Results and Discussion

3.1. Geometric Structure

The structure of the relaxed $Au_{70}S_{20}(PCH_3)_{12}$ cluster is given in Figure 1b, which is in D_2 symmetry. The structural parameters computed here reproduce well with the experimental results.

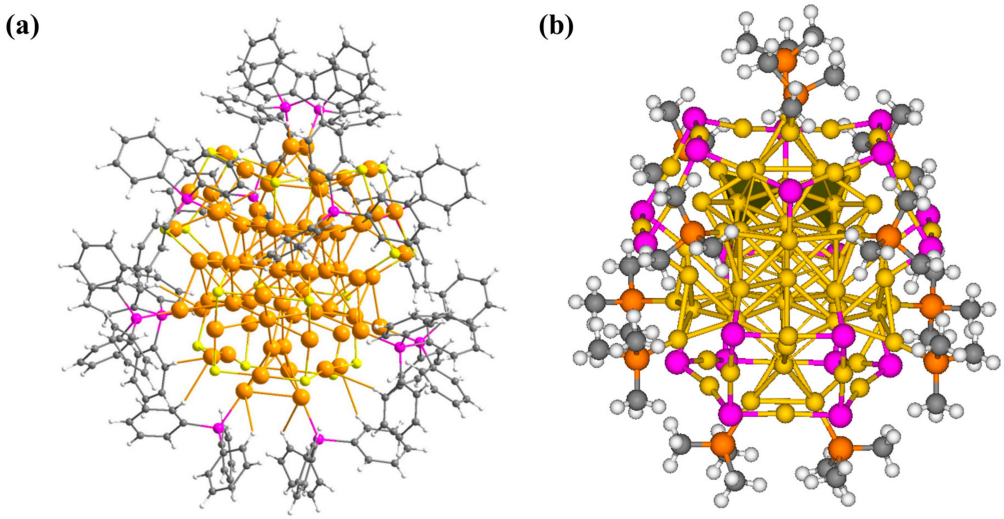

Figure 1. (**a**) Single crystal XRD structure of $Au_{70}S_{20}(PPh_3)_{12}$ from [21], reproduced with permission, Royal Society of Chemistry, 2017; (**b**) The optimized structure of $Au_{70}S_{20}(PCH_3)_{12}$ cluster. The cluster is obtained at the PBE0/LanL2dz(Au) and 6-31G *(S, C, P, H) level of theory. Au, yellow, S, purple; P, orange; C, gray, H, white.

Based on the divide-and-protect concept [22], different building blocks were tried to find the proper segmentation mode. The cluster can be viewed as Au-core and protecting motifs. Through analysis on the structure, the protecting motifs include twelve separate PCH_3 and $(Au\text{-}S)_n$ motifs. According to the segmentation analysis in Supplementary Materials, $Au_{70}S_{20}(PCH_3)_{12}$ cluster is divided into three parts as Figures 2 and 3 show. $Au_{70}S_{20}(PCH_3)_{12}$ cluster can be written as $Au_{70}S_{20}(PCH_3)_{12} = [Au_{46}{}^{16+}][Au_{12}(\mu_3\text{-}S)_{10}{}^{8-}]_2[PCH_3]_{12}$. The core of the cluster is $Au_{46}{}^{16+}$ with two new $[Au_{12}(\mu_3\text{-}S)_{10}]^{8-}$ staple motifs and 12 PCH_3 protecting it. The $[Au_{12}(\mu_3\text{-}S)_{10}]^{8-}$ staple motif containing ten μ_3-S atoms is observed for the first time in Au-L clusters. As shown in Figures 2c and 3c, $[Au_{12}(\mu_3\text{-}S)_{10}]^{8-}$ motif can be easily identified from the cluster. Worth noting is that $[Au_{12}(\mu_3\text{-}S)_{10}]^{8-}$ motif has six branches, which is obviously different from common staple motif and it is unprecedented in $Au_m(SR)_n$ clusters. Each S atom is triply coordinated to the neighboring Au atoms in a μ_3 bridging form. $[Au_{12}(\mu_3\text{-}S)_{10}]^{8-}$ motif has six S legs, thus we term it six-tooth staple motif. According to the theoretical studies by Jiang et al., other motifs than common staple motifs may exist [42]. Moreover, Au_xS_y unit is theoretically predicted existing in core-shell structures of Au_mS_n clusters [43,44]. $[Au_{12}S_8]^{4-}$ anion presented in the

synthesized crystal thioaurate $[Ph_4As]_4[Au_{12}S_8]$. The framework of $[Au_{12}S_8]^{4-}$ anion is a distorted cube, moreover, sulfur, and gold atoms locate at the corners and edge midpoints of the cubic structure, respectively [45].

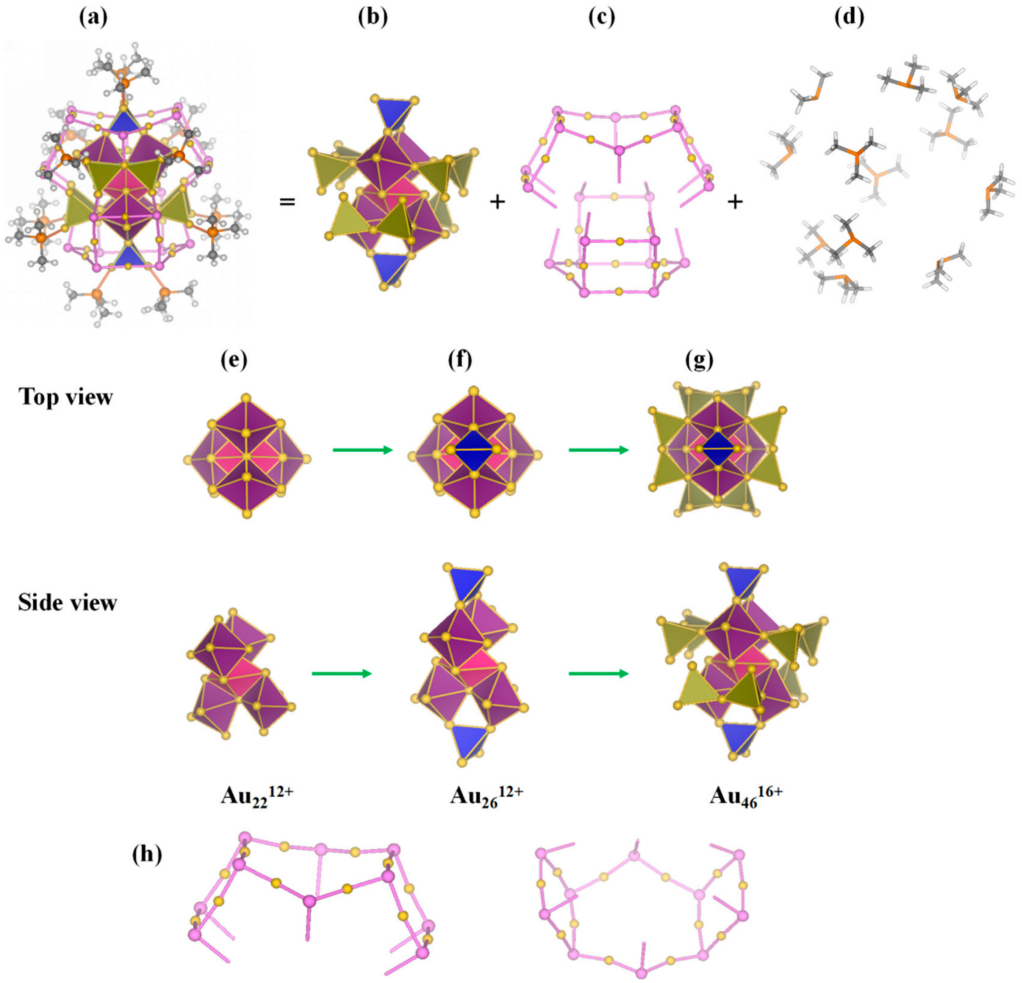

Figure 2. (**a**) Structural model of $Au_{70}S_{20}(PCH_3)_{12}$. The $[Au_{12}(\mu_3\text{-}S)_{10}]^{8-}$ and PCH_3 protecting motifs are given as ball-and-stick models (Au, yellow; P, orange; S, pink; C, gray; H, white). The Au cores are shown as polyhedra. (**b**) Model of Au_{46}^{16+} core, (**c**) Two $[Au_{12}(\mu_3\text{-}S)_{10}]^{8-}$ six-tooth staple motifs, (**d**) Model of twelve PCH_3 protecting motif, (**e**) 6 × 2e SAN of Au_{22}^{12+} core, (**f**) Au_{26}^{12+} core, (**g**) Au_{46}^{16+} core, (**h**) Two views of $[Au_{12}(\mu_3\text{-}S)_{10}]^{8-}$ staple motif.

The $Au_3(\mu_3\text{-}S)$ unit has been proposed as an elementary block and used to design a group of quasi-fullerence hollow-cage $[Au_{3n}(\mu_3\text{-}S)_{2n}]^{n-}$ clusters with high stability [46]. $[Au_{12}(\mu_3\text{-}S)_{10}]^{8-}$ motif can be viewed as a part of $[Au_{15}(\mu_3\text{-}S)_{10}]^{5-}$ cluster, which is a half cage. Here, $[Au_{12}(\mu_3\text{-}S)_{10}]^{8-}$ six-tooth staple motif as a whole protects Au_{46}^{16+} core. The configuration of the vertex-sharing Au_7 core in Au_{46}^{16+} core resembles those in $Au_{28}(SR)_{20}$ and $Au_{20}(SR)_{16}$ clusters [34,47]. From Figure 2, Au_{46}^{16+} core is composed of five edge-sharing Au_6, four vertex-sharing Au_7 and two Au_4 superatoms. The five Au_6 superatoms compose an Au_{22}^{12+} kernel. The valence electrons of Au_{22}^{12+} core is 10e, which is also a 10e superatomic molecule (Figures 1c and 3).

From Figure 2, we can see that the 12 terminal S legs in two $[Au_{12}(\mu_3\text{-}S)_{10}]^{8-}$ staple motifs connect to the neighboring Au_7 cores. The two $[Au_{12}(\mu_3\text{-}S)_{10}]^{8-}$ motifs protect Au_{46}^{16+} core from both top and bottom sides stabilizing the cluster. The average bond length of Au-S in $[Au_{12}(\mu_3\text{-}S)_{10}]^{8-}$ is 2.39 Å suggesting a covalent single bond. The average bond angle of ∠Au-S-Au is 94.7° and thus deviate only

slightly from the ideal 90° expected for bonding involving the sulfur 3p orbitals. Gold attempts to maintain linearity with average bond angle of ∠S-Au-S being 171.4°.

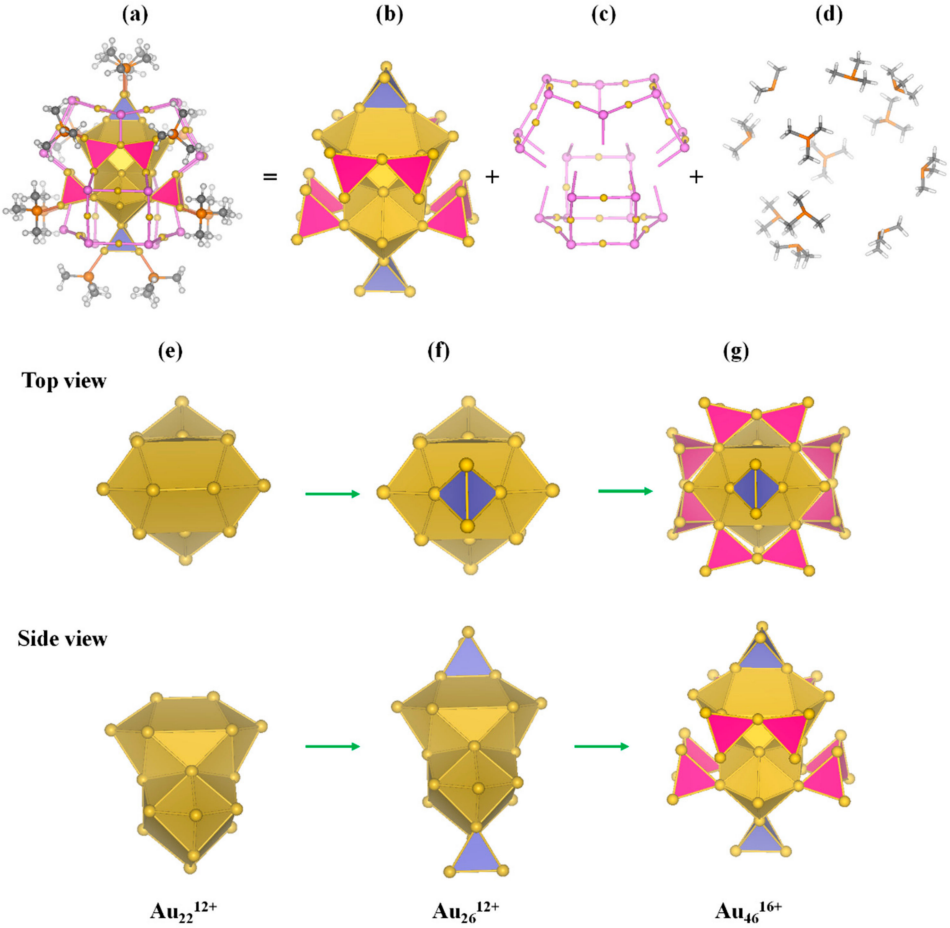

Figure 3. (**a**) Structural model of $Au_{70}S_{20}(PCH_3)_{12}$. The $[Au_{12}(\mu_3\text{-}S)_{10}]^{8-}$ and PCH_3 protecting motifs are given as ball-and-stick models (Au, yellow; P, orange; S, pink; C, gray; H, white). The Au cores are shown as polyhedra. (**b**) Model of Au_{46}^{16+} core, (**c**) Two $[Au_{12}(\mu_3\text{-}S)_{10}]^{8-}$ staple motifs, (**d**) Model of twelve PCH_3 protecting motif, (**e**) Au_{22}^{12+} superatomic molecule, (**f**) Au_{26}^{12+} core, (**g**) Au_{46}^{16+} core.

Figure S1 gives Au–Au contacts in the optimized structure of $Au_{70}S_{20}(PCH_3)_{12}$ cluster: (a) Au_{22} innermost core is 5 × 2e SAN, (b) Au_{22} innermost core is a 10e-superatomic molecule. Also given are the aurophilic contacts between motifs and superatoms and the aurophilic contacts between superatoms. Noticeable gold–gold interactions (baby blue and black lines in Figure S1a,b, Supporting Materials) between the Au atoms in $[Au_{12}(\mu_3\text{-}S)_{10}]^{8-}$ and neighboring gold cores are present. The Au–Au aurophilic distances range from 2.82–3.01 Å, with the average Au–Au distance being 2.91 Å smaller than the Au–Au van der Waals radii (3.32 Å) [48,49]. The blue lines in Figure S1a label the aurophilic interactions between Au_6 and Au_4 cores, and the interactions between Au_4 cores. The green lines in Figure S1b label the aurophilic interactions between Au_{22} and neighboring Au_4 cores. The Au–Au distances range from 2.86–3.01 Å, and the average Au–Au distance is 2.93 Å. The short bond distance between Au and Au indicates strong aurophilic interactions. Thus, the interaction mode between six-tooth staple motifs and Au cores includes clamping and aurophilic interactions, which stabilize the $Au_{70}S_{20}(PCH_3)_{12}$ cluster. Here, the staple motif can extend to six-tooth mode. The staple motif only includes Au and S elements, which is obviously different from previous staple motifs. From above analysis, we can see that both the position of the six-tooth staple motifs and Au–Au contacts in the cluster dedicate to the stability of $Au_{70}S_{20}(PCH_3)_{12}$ cluster.

3.2. Chemical Bonding Analysis

In order to verify the electronic structure of $Au_{70}S_{20}(PCH_3)_{12}$ cluster, we carried out chemical bonding analysis. The electronic structure of the cluster followed the SAN model, that is, it had a network of fifteen 2e-superatoms, abbreviated as 15 × 2e SAN, which contained five 2e-Au_6 and ten 2e-Au_4 superatoms. We took the Au_{46}^{16+} core out of the cluster separately while keeping the structure identical to that in $Au_{70}S_{20}(PCH_3)_{12}$ cluster to analyze the chemical bonds. As expected, AdNDP analysis in Figure 4 indicated that there are 10 four-center-two-electron (4c–2e) bonds with occupancy numbers (ON) = 1.54−1.56 |e|, five 6c−2e bonds with ONs = 1.63−1.68 |e|. Vertex-sharing Au_4 superatoms were present in the experimentally determined $Au_{20}(SR)_{16}$ and $Au_{36}(SR)_{24}$ clusters [33,34].

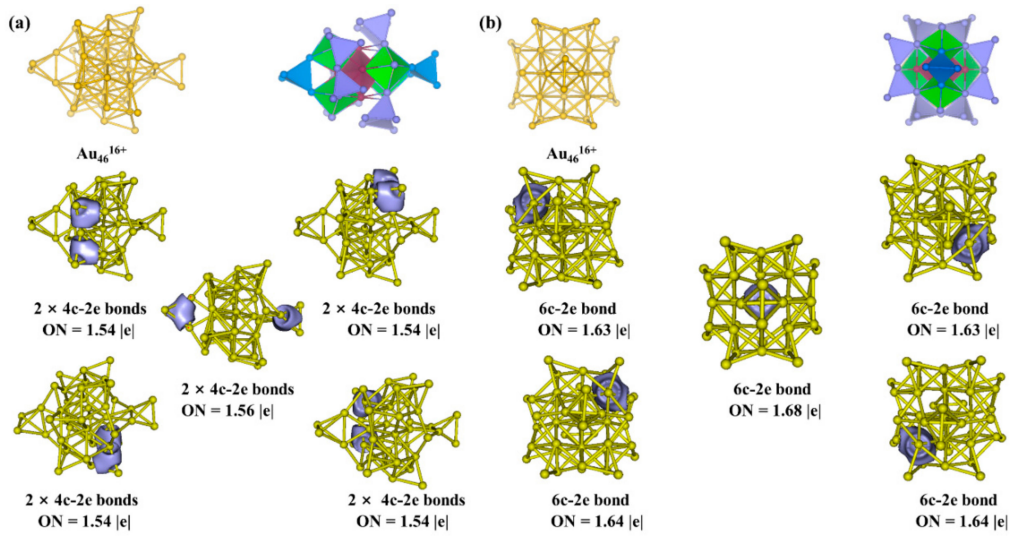

Figure 4. Structures, superatom-network models and adaptive natural density partitioning (AdNDP) localized natural bonding orbitals of (**a**) 4**c**–2**e** bonds (side view), (**b**) 6**c**–2**e** bonds (top view) in Au_{46}^{16+} core of $Au_{70}S_{20}(PCH_3)_{12}$ cluster.

For purposes of confirming the segmentation scheme, the difference of Au–Au distances inside the Au_{46} core and those between Au_{46} core and two six-tooth staple motifs were recorded. Figure S2 (Supporting Materials) displays all the Au–Au distances, which include the distances between Au_{46} core and two six-tooth staple motifs (black dots), the Au–Au distances in Au_{22} core (red dots), in two Au_4 superatoms on top and bottom of the cluster (blue dots), in the four pairs of vertex-sharing Au_4 superatoms (purple dots). The average Au–Au distances of the above four groups were 2.90, 2.91, 2.82, and 2.86 Å, respectively. From the figure, we can see that, the Au–Au distances between Au_{46} core and two six-tooth staple motifs and distances in the Au_{22} core were relatively bigger than other two groups. The Au_{22} core was consistent with the former report [21]. The reason for the Au–Au distances in Au_{22} core being relatively bigger are probably that the repulsive interactions of Au atoms can be reduced in this way. Lower repulsion is helpful to form a Au_{22} core. The Au–Au distances in the ten Au_4 superatoms were shorter than those between the Au-core and staple motifs, which follow the concept of SAN model. The shorter Au–Au distances were helpful to the formation of Au_4 superatoms. In short, the existence of ten Au_4 superatoms were reasonable, which has been supported from the viewpoint of Au–Au distances.

Further analysis of the innermost Au_{22}^{12+} core was performed and the structure of Au_{22}^{12+} core stayed the same as that in Au_{46}^{16+} core. The results are given in Figure 5. From Figure 5a, we can see that Au_{22}^{12+} core can be viewed as five edge-sharing Au_6 superatoms. AdNDP analysis confirms that there are five 6c–2e bonds. ON is 1.83 |e| for the middle 6c–2e bond, while ONs are all 1.77 |e| for the marginal 6c–2e bonds. The Au_9 kernel in $Au_{18}(SR)_{14}$ cluster consists of two Au_6 superatoms [50,51]. Au_{22}^{12+} core has 10 valence electrons which is identical to a N_2 molecule, and it can be viewed as a

super-N_2 molecule. From Figure 5b, AdNDP analysis demonstrates that Au_{22}^{12+} has two 11c–2e super 1S lone pairs with ONs being 1.91 |e|, one 22c–2e super-σ bond and two 22c–2e super π bonds with ONs being 2.00 |e|.

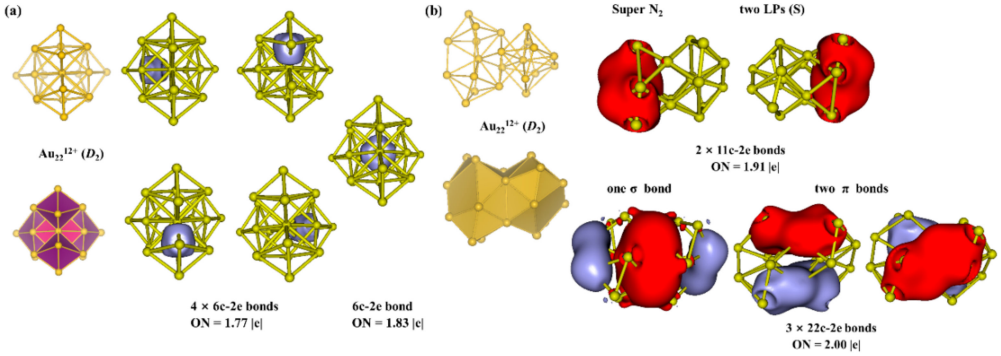

Figure 5. (**a**) Structure, superatom-network model and AdNDP localized natural bonding orbitals of Au_{22}^{12+} core. (**b**) Structure, superatomic molecular model and AdNDP localized natural bonding orbitals of Au_{22}^{12+} superatomic molecule.

3.3. Aromatic Analysis

NICS-scan method is proposed by Stanger, which is similar to the screen method of aromatic center and has been used to predict the aromatic properties of molecules and clusters [52–54]. Here, we use NICS-scan method to further verify the existence of Au_4 superatoms and we have demonstrated the existence of Au_4 superatoms in $Au_{20}(SR)_{16}$, $Au_{28}(SR)_{20}$ and $Au_{30}S_2(SR)_{18}$ clusters in our former work [19,36]. Figure 6 is the NICS-scan curve of Au_{46}^{16+} core along the centers of two neighboring Au_4 superatoms in the range of −6.0–6.0 Å. The position of NICS(0) is set at the midpoint of the geometric centers of two Au_4 superatoms. Two views of the scan in Au_{46}^{16+} have been given in the figure. Considering the symmetry of Au_{46}^{16+}, we only give one scan curve of the cluster. It is obvious that there are two dotted ovals in the figure, indicating two non-conjugate Au_4 superatoms, which further support the SAN model. The NICS(0) values of the two Au_4 superatoms are both −32.2 ppm much smaller than benzene molecule (−9.7 ppm), indicating strong aromaticity. The NICS-scan method is applied to verify Au_4 superatoms in Au_{46}^{16+} core, thus the Au_4 superatoms are further verified from the aromatic view.

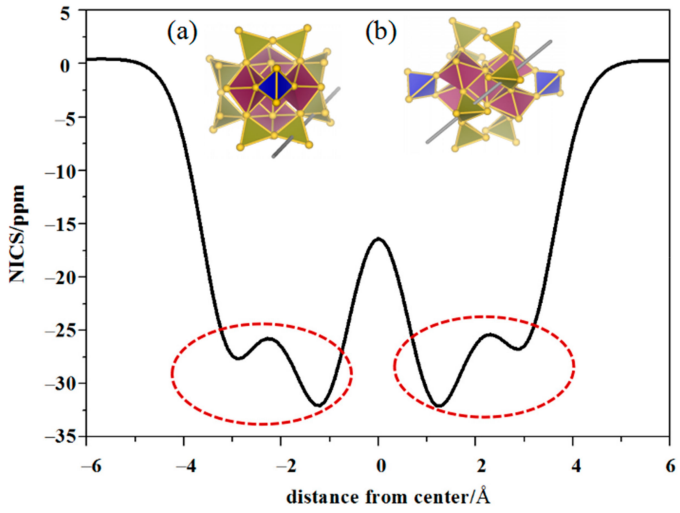

Figure 6. NICScc-scan curve of the Au_{46}^{16+} core, which is the scan along the centers of the neighboring Au_4 superatoms in the range of –6.0–6.0 Å. The red dotted ovals in the figure signal the presence of Au_4 superatoms. The structures labeled in (**a**) and (**b**) indicate two views of the scan.

3.4. $Cu_6@Au_{12}(\mu_3\text{-}S)_8$, $Ag_6@Au_{12}(\mu_3\text{-}S)_8$, and $Au_6@Au_{12}(\mu_3\text{-}S)_8$ Clusters

Worth noting is that $[Au_{12}(\mu_3\text{-}S)_8]^{4-}$ was experimentally crystallized earlier [45]. Meanwhile, the structure of $[Au_{12}(\mu_3\text{-}S)_8]^{4-}$ was theoretically studied [46]. We obtained the optimized structure and harmonic frequencies of $[Au_{12}(\mu_3\text{-}S)_8]^{4-}$ cluster at the level of PBE0/Lanl2dz(Au), 6-31G *(S). The optimized structure presented a cubic structure in O_h symmetry and the Au-S bond length is 2.38 Å. It was found that the harmonic vibrational frequencies of $[Au_{12}(\mu_3\text{-}S)_8]^{4-}$ were all positive. The HOMO-LUMO gap was 2.90 eV, further indicating its high stability.

Jiang et al. have predicted several core-in-cage gold sulfide $Au_xS_y^-$ clusters observed in MALDI fragmentation of $Au_{25}(SR)_{18}^-$ cluster theoretically [42]. They stated that the Au core in the core-in-cage cluster may catalyze reactions. Inspired by the half-cage $[Au_{12}(\mu_3\text{-}S)_{10}]^{8-}$ staple motif, the cubic $[Au_{12}(\mu_3\text{-}S)_8]^{4-}$ cluster can be regarded as a cage staple motif. Thus, we designed three core-in-cage clusters, $Cu_6@Au_{12}(\mu_3\text{-}S)_8$, $Ag_6@Au_{12}(\mu_3\text{-}S)_8$, and $Au_6@Au_{12}(\mu_3\text{-}S)_8$. The structures, models and AdNDP analysis of the three designed clusters are collected in Figure 7. The core-in-cage clusters can keep O_h symmetry after relaxation. The harmonic vibrational frequencies of the three clusters are all positive, indicating they are real local minima on potential energy surfaces. The infrared spectrograms (IR) of them are given in Figure S3. The HOMO-LUMO gaps of $Cu_6@Au_{12}(\mu_3\text{-}S)_8$, $Ag_6@Au_{12}(\mu_3\text{-}S)_8$, and $Au_6@Au_{12}(\mu_3\text{-}S)_8$ clusters are 3.59, 2.97, and 2.87 eV, suggesting their high stability. $Cu_6@Au_{12}(\mu_3\text{-}S)_8$ is more stable than other two clusters because Ag_6 and Au_6 are too large. The Cu–Au, Ag–Au and Au–Au distances between the atoms in core and cage of the three clusters are 2.63, 2.74 and 2.74 Å (Figure 7), respectively. All of them are smaller than the sum of their van der Waals radii (3.12, 3.38, and 3.32 Å) [55], demonstrating that Cu–Au, Ag–Au, and Au–Au interactions play a dominant role in stabilizing the clusters. The cores of the designed clusters are all-metal, which are reminiscent of all-metal aromatic. Thus it is necessary to calculate the NICS(0) values to evaluate the stabilities. The NICS(0) values of $Cu_6@Au_{12}(\mu_3\text{-}S)_8$, $Ag_6@Au_{12}(\mu_3\text{-}S)_8$, and $Au_6@Au_{12}(\mu_3\text{-}S)_8$ are −19.6, −17.0, and −17.9 ppm, respectively. The largely negative NICS(0) values of the cores exhibit that they are aromatic and stable. The aromaticity of the centers contributes to the stabilities of the clusters.

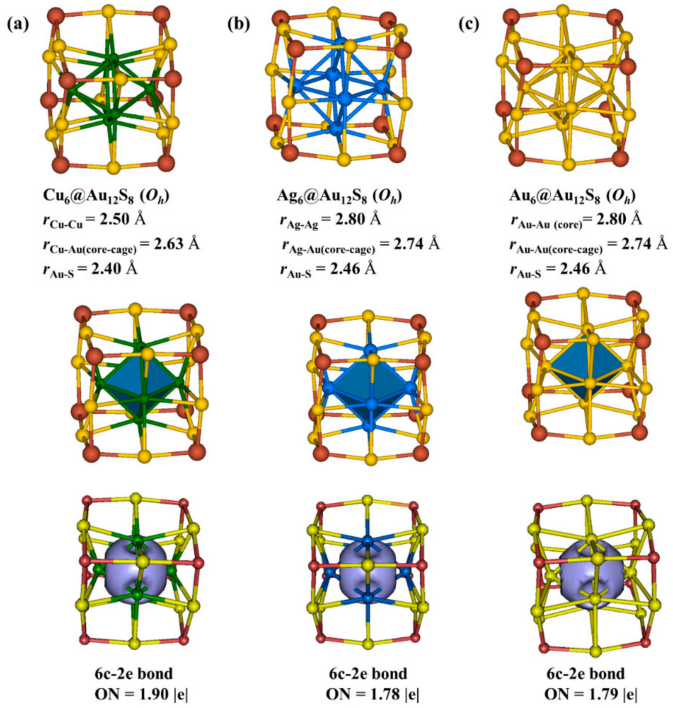

Figure 7. Structures, superatom models and AdNDP localized natural bonding orbitals of 6c-2e bonds in (**a**) $Cu_6@Au_{12}(\mu_3\text{-}S)_8$, (**b**) $Ag_6@Au_{12}(\mu_3\text{-}S)_8$, and (**c**) $Au_6@Au_{12}(\mu_3\text{-}S)_8$ clusters. Cu, green; Ag, blue; Au, yellow; S, brown.

In order to study the thermodynamic stability of the $Cu_6@Au_{12}(\mu_3\text{-}S)_8$, $Ag_6@Au_{12}(\mu_3\text{-}S)_8$ and $Au_6@Au_{12}(\mu_3\text{-}S)_8$ clusters, $Cu_6@Au_{12}(\mu_3\text{-}S)_8$ cluster is taken as a test case. The thermodynamic stabilities of $Cu_6@Au_{12}(\mu_3\text{-}S)_8$ cluster is further confirmed by ab initio molecular dynamics (AIMD) simulations. The AIMD studies of the cluster is carried out using Vienna ab initio simulation package (VASP) with PBE0 method [39,56]. Four different temperatures at 300, 500, 700, and 1000 K with a simulation time of 8ps have been performed. The AIMD simulations of $Cu_6@Au_{12}(\mu_3\text{-}S)_8$ cluster are plotted in Figure S4. From the figure, it is obvious that the structure of $Cu_6@Au_{12}(\mu_3\text{-}S)_8$ cluster can keep after simulation in the temperature range of 300–1000 K, indicating its high thermostability.

The chemical bonding patterns of the three clusters have been analyzed. According to the results of AdNDP analysis (see Figure S5), each $M_6@Au_{12}(\mu_3\text{-}S)_8$ (M = Cu, Ag, and Au) cluster has 24 2c-2e Au-S σ bonds with ONs being 1.85, 1.83 and 1.82 |e|, respectively. From Figure 7, each cluster has one 6c–2e bond, and occupancy numbers of the three 6c–2e bonds in $Cu_6@Au_{12}(\mu_3\text{-}S)_8$, $Ag_6@Au_{12}(\mu_3\text{-}S)_8$ and $Au_6@Au_{12}(\mu_3\text{-}S)_8$ are 1.90, 1.78, and 1.79 |e|, respectively.

4. Conclusions

In conclusion, we have explored the electronic and geometric structure of the recently determined $Au_{70}S_{20}(PPh_3)_{12}$ cluster on the basis of the divide-and-protect concept and SAN model. $Au_{70}S_{20}(PPh_3)_{12}$ cluster is a 30e-compound, which does not satisfy the magic number of SAC concept. Based on SAN model, the cluster has fifteen 2e-superatoms. The $Au_{46}{}^{16+}$ core is composed of one $Au_{22}{}^{12+}$ innermost core and ten surrounding 2e-Au_4 superatoms. The $Au_{22}{}^{12+}$ innermost core can either be viewed as a network of five 2e-Au_6 superatoms, or be considered as a 10e-superatomic molecule. When $Au_{22}{}^{12+}$ innermost core is viewed as a network of five 2e-Au_6 superatoms, the $Au_{46}{}^{16+}$core can be described as a 15 × 2e SAN consisting of 10 × 2e Au_4 and 5 × 2e Au_6 superatoms. The vertex-sharing Au_7 core exists in the experimentally determined $Au_{20}(SR)_{16}$ and $Au_{36}(SR)_{24}$ clusters. A new branching staple motif, six-tooth staple motif, $[Au_{12}(\mu_3\text{-}S)_{10}]^{8-}$, is discovered in Au-L clusters for the first time. The six-tooth staple motif is obviously different from common staple motifs, which have six S legs. Here the newly discovered staple motif enriches the staple motif family. The NICS-san method has been used to confirm the presence of Au_4 superatoms. The new segmentation method here can properly explain the structure and stability of $Au_{70}S_{20}(PPh_3)_{12}$ cluster. The reason for the stability and the nature of bonds have been given. Concretely, the six-tooth staple motifs, the superatom network, the aromatic of the superatoms and Au–Au interactions contribute to the stability of the cluster. We have designed three core-in-cage $Cu_6@Au_{12}(\mu_3\text{-}S)_8$, $Ag_6@Au_{12}(\mu_3\text{-}S)_8$, and $Au_6@Au_{12}(\mu_3\text{-}S)_8$ clusters based on $[Au_{12}(\mu_3\text{-}S)_8]^{4-}$. The three clusters are stable in O_h symmetry. Each of them has one 6c-2e bond in the core. Aromatic analysis reveals that they are aromatic molecules. The $[Au_{12}(\mu_3\text{-}S)_8]^{4-}$ cluster has been experimentally synthesized, and the three constructed clusters are stable based on our computation, thus the three designed clusters may be synthesized in future. Our work will provide some new perspectives to the electronic structure and stability of $Au_{70}S_{20}(PPh_3)_{12}$ cluster. The concept of half-cage and cage staple motif could offer some reference to future synthesis of Au-L clusters.

Supplementary Materials: The following are available online at http://www.mdpi.com/2079-4991/9/8/1132/s1, The segmentation method of $Au_{70}S_{20}(PCH_3)_{12}$ cluster. Figure S1: The Au–Au contacts in the optimized structure of $Au_{70}S_{20}(PCH_3)_{12}$ cluster. (a) Au_{22} innermost core is 5 × 2e SAN, (b) Au_{22} innermost core is a 10e-superatomic molecule. The baby blue and black lines in the structure indicate aurophilic contacts between motifs and superatoms, while blue and green lines show aurophilic contacts between superatoms. Figure S2: (a) The Au–Au bond distances between Au_{46} core and staple motifs, (b) the Au–Au distances in Au_{22} core, (c) the Au–Au distances in two Au_4 superatoms on top and bottom of the cluster, (d) the Au–Au distances in the four pairs of vertex-sharing Au_4 superatoms. Figure S3: IR spectra of $Cu_6@Au_{12}(\mu_3\text{-}S)_8$, $Ag_6@Au_{12}(\mu_3\text{-}S)_8$ and $Au_6@Au_{12}(\mu_3\text{-}S)_8$ clusters. Figure S4: Geometric configuration of $Cu_6@Au_{12}(\mu_3\text{-}S)_8$ at after 8 ps AIMD simulations at (a) 300 K, (b) 500 K, (c) 700 K and (d) 1000 K, respectively. Cu, green; Au, yellow; S, brown. Figure S5: Geometries (Cu, green; Ag, blue; Au, yellow) and AdNDP localized natural bonding orbitals of Au-S σ-bonds in (a) $Cu_6@Au_{12}(\mu_3\text{-}S)_8$, (b) $Ag_6@Au_{12}(\mu_3\text{-}S)_8$ and (c) $Au_6@Au_{12}(\mu_3\text{-}S)_8$ clusters.

Author Contributions: Density functional theory (DFT) computations, Z.M.T.; data analysis, Z.M.T. and L.J.C., writing—original draft preparation, Z.M.T; writing—review and editing, Z.M.T. and L.J.C.; supervision, L.J.C.

Funding: This research was funded by the National Natural Science Foundation of China (21873001), the Foundation of Distinguished Young Scientists of Anhui Province and the financial support of the Fuyang Normal University (2017FSKJ01ZD).

Acknowledgments: The authors acknowledge the high-performance computing center of Anhui university.

Conflicts of Interest: The authors declare no conflict of interest.

References

1. Jadzinsky, P.D.; Calero, G.; Ackerson, C.J.; Bushnell, D.A.; Kornberg, R.D. Structure of a thiol monolayer-protected gold nanoparticle at 1.1 Å resolution. *Science* **2007**, *318*, 430–433. [CrossRef]
2. Zhu, M.Z.; Aikens, C.M.; Hollander, F.J.; Schatz, G.C.; Jin, R.C. Correlating the crystal structure of a thiol-protected Au_{25} cluster and optical properties. *J. Am. Chem. Soc.* **2008**, *130*, 5883–5885. [CrossRef] [PubMed]
3. Yuan, S.F.; Li, P.; Tang, Q.; Wan, X.K.; Nan, Z.A.; Jiang, D.E.; Wang, Q.M. Alkynyl-protected silver nanoclusters featuring an anticuboctahedral kernel. *Nanoscale* **2017**, *9*, 11405–11409. [CrossRef] [PubMed]
4. Das, A.; Li, T.; Nobusada, K.; Zeng, C.; Rosi, N.L.; Jin, R.C. Nonsuperatomic $[Au_{23}(SC_6H_{11})_{16}]^-$ nanocluster featuring bipyramidal Au_{15} kernel and trimeric $Au_3(SR)_4$ motif. *J. Am. Chem. Soc.* **2013**, *135*, 18264–18267. [CrossRef] [PubMed]
5. Dass, A.; Theivendran, S.; Nimmala, P.R.; Kumara, C.; Jupally, V.R.; Fortunelli, A.; Sementa, L.; Barcaro, G.; Zuo, X.B.; Noll, B.C. $Au_{133}(SPh\text{-}tBu)_{52}$ nanomolecules: X-ray crystallography, optical, electrochemical, and theoretical Analysis. *J. Am. Chem. Soc.* **2015**, *137*, 4610–4613. [CrossRef] [PubMed]
6. Li, Y.F.; Chen, M.; Wang, S.X.; Zhu, M.Z. Intramolecular metal exchange reaction promoted by thiol ligands. *Nanomaterials* **2018**, *8*, 1070. [CrossRef] [PubMed]
7. Pei, Y.; Gao, Y.; Shao, N.; Zeng, X.C. Thiolate-protected Au_{20} $(SR)_{16}$ cluster: Prolate Au_8 core with new $[Au_3(SR)_4]$ staple motif. *J. Am. Chem. Soc.* **2009**, *131*, 13619–13621. [CrossRef]
8. Pei, Y.; Tang, J.; Tang, X.Q.; Huang, Y.Q.; Zeng, X.C. New structure model of $Au_{22}(SR)_{18}$: Bitetrahederon golden kernel enclosed by $[Au_6(SR)_6]$ Au(I) complex. *J. Phys. Chem. Lett.* **2015**, *6*, 1390–1395. [CrossRef]
9. Jiang, D.E.; Walter, M.; Akola, J. On the structure of a thiolated gold cluster: $Au_{44}(SR)_{28}^{2-}$. *J. Phys. Chem. C* **2010**, *114*, 15883–15889. [CrossRef]
10. Malola, S.; Lehtovaara, L.; Knoppe, S.; Hu, K.J.; Palmer, R.E.; Bürgi, T.; Häkkinen, H. $Au_{40}(SR)_{24}$ cluster as a chiral dimer of 8-electron superatoms: Structure and optical properties. *J. Am. Chem. Soc.* **2012**, *134*, 19560–19563. [CrossRef]
11. Tlahuice-Flores, A. Ligand effects on the optical and chiroptical properties of the thiolated Au_{18} cluster. *Phys. Chem. Chem. Phys.* **2016**, *18*, 27738–27744. [CrossRef] [PubMed]
12. Muñoz-Castro, A.; Maturana, R.G. Understanding planar ligand-supported MAu_5 and MAu_6 cores. Theoretical survey of $[MAu_5(Mes)_5]$ and $[MAu_6(Mes)_6]$ (M = Cu, Ag, Au; Mes = 2, 4, 6-$Me_3C_6H_2$) under the planar superatom model. *J. Phys. Chem. C* **2014**, *118*, 21185–21191. [CrossRef]
13. Jin, R.C.; Zeng, C.J.; Zhou, M.Z.; Chen, Y.X. Atomically precise colloidal metal nanoclusters and nanoparticles: Fundamentals and opportunities. *Chem. Rev.* **2016**, *116*, 10346–10413. [CrossRef] [PubMed]
14. Jones, T.C.; Sementa, L.; Stener, M.; Gagnon, K.J.; Thanthirige, V.D.; Ramakrishna, G.; Fortunelli, A.; Dass, A. $Au_{21}S(SAdm)_{15}$: Crystal structure, mass spectrometry, optical spectroscopy, and first-principles theoretical analysis. *J. Phys. Chem. C* **2017**, *121*, 10865–10869. [CrossRef]
15. Yang, H.Y.; Wang, Y.; Edwards, A.J.; Yan, J.Z.; Zheng, N.F. High-yield synthesis and crystal structure of a green Au_{30} cluster co-capped by thiolate and sulfide. *Chem. Commun.* **2014**, *50*, 14325–14327. [CrossRef] [PubMed]
16. Crasto, D.; Malola, S.; Brosofsky, G.; Dass, A.; Häkkinen, H. Single crystal XRD structure and theoretical analysis of the chiral $Au_{30}S(S\text{-}t\text{-}Bu)_{18}$ cluster. *J. Am. Chem. Soc.* **2014**, *136*, 5000–5005. [CrossRef] [PubMed]
17. Liu, C.; Li, T.; Li, G.; Nobusada, K.; Zeng, C.J.; Pang, G.; Rosi, N.L.; Jin, R.C. Observation of body-centered cubic gold nanocluster. *Angew. Chem. Int. Ed.* **2015**, *54*, 9826–9829. [CrossRef]
18. Higaki, T.; Liu, C.; Zhou, M.; Luo, T.Y.; Rosi, N.L.; Jin, R.C. Tailoring the structure of 58-electron gold nanoclusters: $Au_{103}S_2(S\text{-}Nap)_{41}$ and its implications. *J. Am. Chem. Soc.* **2017**, *139*, 9994–10001. [CrossRef] [PubMed]

19. Tian, Z.M.; Cheng, L.J. Electronic and geometric structures of Au_{30} clusters: A network of 2e-superatom Au cores protected by tridentate protecting motifs with μ_3-S. *Nanoscale* **2016**, *8*, 826–834. [CrossRef] [PubMed]
20. Kenzler, S.; Schrenk, C.; Schnepf, A. $Au_{108}S_{24}(PPh_3)_{16}$: A highly symmetric nanoscale gold cluster confirms the general concept of metalloid clusters. *Angew. Chem. Int. Ed.* **2017**, *56*, 393–396. [CrossRef]
21. Kenzler, S.; Schrenk, C.; Frojd, A.R.; Hakkinen, H.; Clayborne, A.Z.; Schnepf, A. $Au_{70}S_{20}(PPh_3)_{12}$: An intermediate sized metalloid gold cluster stabilized by the Au_4S_4 ring motif and Au-PPh_3 groups. *Chem. Commun.* **2018**, *54*, 248–251. [CrossRef] [PubMed]
22. Häkkinen, H.; Walter, M.; Grönbeck, H. Divide and protect: Capping gold nanoclusters with molecular gold-thiolate rings. *J. Phys. Chem. B* **2006**, *110*, 9927–9931. [CrossRef] [PubMed]
23. Heaven, M.W.; Dass, A.; White, P.S.; Holt, K.M.; Murray, R.W. Crystal structure of the gold nanoparticle $[N(C_8H_{17})_4]$ $[Au_{25}(SCH_2CH_2Ph)_{18}]$. *J. Am. Chem. Soc.* **2008**, *130*, 3754–3755. [CrossRef] [PubMed]
24. Pei, Y.; Gao, Y.; Zeng, X.C. Structural prediction of thiolate-protected Au_{38}: A face-fused bi-icosahedral Au core. *J. Am. Chem. Soc.* **2008**, *130*, 7830–7832. [CrossRef] [PubMed]
25. Lopez-Acevedo, O.; Akola, J.; Whetten, R.L.; Gronbeck, H.; Häkkinen, H. Structure and bonding in the ubiquitous icosahedral metallic gold cluster $Au_{144}(SR)_{60}$. *J. Phys. Chem. C* **2009**, *113*, 5035–5038. [CrossRef]
26. Knoppe, S.; Wong, O.A.; Malola, S.; Häkkinen, H.; Bürgi, T.; Verbiest, T.; Ackerson, C.J. Chiral phase transfer and enantioenrichment of thiolate-protected Au_{102} clusters. *J. Am. Chem. Soc.* **2014**, *136*, 4129–4132. [CrossRef]
27. Xu, W.W.; Gao, Y.; Zeng, X.C. Unraveling structures of protection ligands on gold nanoparticle $Au_{68}(SH)_{32}$. *Sci. Adv.* **2015**, *1*, e1400211. [CrossRef] [PubMed]
28. Xu, W.W.; Li, Y.; Gao, Y.; Zeng, X.C. Medium-sized $Au_{40}(SR)_{24}$ and $Au_{52}(SR)_{32}$ nanoclusters with distinct gold-kernel structures and spectroscopic features. *Nanoscale* **2016**, *8*, 1299–1304. [CrossRef]
29. Xiong, L.; Peng, B.; Ma, Z.; Wang, P.; Pei, Y. A ten-electron (10e) thiolate-protected $Au_{29}(SR)_{19}$ cluster: Structure prediction and a 'gold-atom insertion, thiolate-group elimination' mechanism. *Nanoscale* **2017**, *9*, 2895–2902. [CrossRef]
30. Xu, W.W.; Zhu, B.; Zeng, X.C.; Gao, Y. A grand unified model for liganded gold clusters. *Nat. Commun.* **2016**, *7*, 13574. [CrossRef]
31. Xu, W.W.; Zeng, X.C.; Gao, Y. The structural isomerism in gold nanoclusters. *Nanoscale* **2018**, *10*, 9476–9483. [CrossRef] [PubMed]
32. Ma, Z.Y.; Wang, P.; Xiong, L.; Pei, Y. Thiolate-protected gold nanoclusters: Structural prediction and the understandings of electronic stability from first principles simulations. *WIREs Comput. Mol. Sci.* **2017**, *7*, e1315. [CrossRef]
33. Nimmala, P.R.; Knoppe, S.; Jupally, V.R.; Delcamp, J.H.; Aikens, C.M.; Dass, A. $Au_{36}(SPh)_{24}$ nanomolecules: X-ray crystal structure, optical spectroscopy, electrochemistry, and theoretical analysis. *J. Phys. Chem. B* **2014**, *118*, 14157–14167. [CrossRef] [PubMed]
34. Zeng, C.J.; Liu, C.; Chen, Y.X.; Rosi, N.L.; Jin, R.C. Gold-thiolate ring as a protecting motif in the $Au_{20}(SR)_{16}$ nanocluster and implications. *J. Am. Chem. Soc.* **2014**, *136*, 11922–11925. [CrossRef] [PubMed]
35. Walter, M.; Akola, J.; Lopez-Acevedo, O.; Jadzinsky, P.D.; Calero, G.; Ackerson, C.J.; Whetten, R.L.; Grönbeck, H.; Häkkinen, H. A unified view of ligand-protected gold clusters as superatom complexes. *Proc. Natl. Acad. Sci. USA* **2008**, *105*, 9157–9162. [CrossRef] [PubMed]
36. Cheng, L.J.; Yuan, Y.; Zhang, X.Z.; Yang, J.L. Superatom networks in thiolate-protected gold nanoparticles. *Angew. Chem. Int. Ed.* **2013**, *52*, 9035–9039. [CrossRef] [PubMed]
37. Pei, Y.; Lin, S.S.; Su, J.C.; Liu, C.Y. Structure prediction of $Au_{44}(SR)_{28}$: A chiral superatom cluster. *J. Am. Chem. Soc.* **2013**, *135*, 19060–19063. [CrossRef] [PubMed]
38. Frisch, M.J.; Schlegel, H.B.; Scuseria, G.E.; Robb, M.A.; Cheeseman, J.R.; Scalmani, G.; Barone, V.; Mennucci, B.; Petersson, G.A.; Nakatsuji, H.; et al. *Gaussian 09, Revision B 01*; Gaussian, Inc.: Wallingford, CT, USA, 2009.
39. Perdew, J.P.; Burke, K.; Ernzerhof, M. Generalized gradient approximation made simple. *Phys. Rev. Lett.* **1996**, *77*, 3865–3868. [CrossRef]
40. Zubarev, D.Y.; Boldyrev, A.I. Developing paradigms of chemical bonding: Adaptive natural density partitioning. *Phys. Chem. Chem. Phys.* **2008**, *10*, 5207–5217. [CrossRef]
41. Varetto, U. *MOLEKEL*, version 5.4.0.8; Swiss National Supercomputing Centre: Manno, Switzerland, 2009. Available online: http://ugovaretto.github.io/molekel/wiki/pmwiki.php/Main/HomePage.html (accessed on 1 August 2019).

42. Jiang, D.E.; Walter, M.; Dai, S. Gold sulfide nanoclusters: A unique core-in-cage structure. *Chem. Eur. J.* **2010**, *16*, 4999–5003. [CrossRef]
43. Pei, Y.; Shao, N.; Li, H.; Jiang, D.E.; Zeng, X.C. Hollow polyhedral structures in small gold-sulfide clusters. *ACS Nano* **2011**, *5*, 1441–1449. [CrossRef] [PubMed]
44. Feng, Y.Q.; Cheng, L.J. Structural evolution of $(Au_2S)_n$ (n = 1-8) clusters from first principles global optimization. *RSC Adv.* **2015**, *5*, 62543–62550. [CrossRef]
45. Gerolf, M.; Joachim, S. Synthesis and crystal Structure of $[Ph_4As]_4[Au_{12}S_8]$, a distorted cubane-like thioaurate(I). *Angew. Chem. Int. Ed. Engl.* **1984**, *23*, 715–716. [CrossRef]
46. Xu, W.W.; Zeng, X.C.; Gao, Y. $(Au_3(\mu_3\text{-S})$ (0e) elementary block: New insights into ligated gold clusters with μ_3-sulfido motifs. *Nanoscale* **2017**, *9*, 8990–8996. [CrossRef] [PubMed]
47. Knoppe, S.; Malola, S.; Lehtovaara, L.; Bürgi, T.; Häkkinen, H. Electronic structure and optical properties of the thiolate-protected $Au_{28}(SMe)_{20}$ Cluster. *J. Phys. Chem. A* **2013**, *117*, 10526–10533. [CrossRef]
48. Pyykkö, P.; Mendizabal, F. Theory of d^{10}-d^{10} closed-shell attraction. III. rings. *Inorg. Chem.* **1998**, *37*, 3018–3025. [CrossRef]
49. Pekka, P.; Nino, R.; Fernando, M. Theory of the d^{10}-d^{10} closed-shell attraction: 1. dimers near equilibrium. *Chem. Eur. J.* **1997**, *3*, 1451–1457. [CrossRef]
50. Chen, S.; Wang, S.X.; Zhong, J.; Song, Y.B.; Zhang, J.; Sheng, H.T.; Pei, Y.; Zhu, M.Z. The structure and optical properties of the $[Au_{18}(SR)_{14}]$ nanocluster. *Angew. Chem. Int. Ed.* **2015**, *54*, 3145–3149. [CrossRef]
51. Das, A.; Liu, C.; Byun, H.Y.; Nobusada, K.; Zhao, S.; Rosi, N.; Jin, R.C. Structure determination of $[Au_{18}(SR)_{14}]$. *Angew. Chem.* **2015**, *127*, 3183–3187. [CrossRef]
52. Stanger, A. Nucleus-independent chemical shifts (NICS): Distance dependence and revised criteria for aromaticity and antiaromaticity. *J. Org. Chem.* **2006**, *71*, 883–893. [CrossRef]
53. Tian, Z.M.; Cheng, L.J. First principles study on the structural evolution and properties of $(MCl)_n$ (n = 1–12, M = Cu, Ag) clusters. *RSC Adv.* **2016**, *6*, 30311–30319. [CrossRef]
54. Yuan, Y.; Cheng, L. B_{14}^{2+}: A magic number double-ring cluster. *J. Chem. Phys.* **2012**, *137*, 044308. [CrossRef] [PubMed]
55. Bondi, A. Van der Waals volumes and radii. *J. Phys. Chem.* **1964**, *68*, 441–451. [CrossRef]
56. Kresse, G.; Furthmüller, J. Efficient iterative schemes for ab initio total-energy calculations using a plane-wave basis set. *Phys. Rev. B* **1996**, *54*, 11169–11186. [CrossRef] [PubMed]